SUPPORTING INFORMATION

RNA adapts its flexibility to efficiently fold and resist unfolding

Sukjin S. Jang[1,†,§], Korak Kumar Ray[1,‡,§], David G. Lynall[2,§], Kenneth L. Shepard[2], Colin Nuckolls[1,*], Ruben L. Gonzalez, Jr.[1,*]

[1] *Department of Chemistry, Columbia University, New York, NY 10027 USA*

[2] *Department of Electrical Engineering, Columbia University, New York, NY 10027 USA*

[†] *Current Address: Department of Biological Chemistry and Molecular Pharmacology, Harvard Medical School, Boston, MA 02115 USA*

[‡] *Current Address: MRC-Laboratory of Medical Sciences, London W12 0HS, UK*

[§] These authors contributed equally to this work.

*To whom correspondence may be addressed: Colin Nuckolls, Department of Chemistry, Columbia University, 3000 Broadway, New York, NY 10027, Tel: (212) 854-6289, Email: cn37@columbia.edu.; Ruben L. Gonzalez, Jr., Department of Chemistry, Columbia University, 3000 Broadway, New York, NY 10027, Tel: (212) 854-1096, Email: rlg2118@columbia.edu

Conductance trajectories arise from the zipping dynamics of a single stem-loop

To validate that the observed conductance trajectories in our experiments arise from the zipping dynamics of a single, surface-tethered stem-loop RNA, we first determined the ensemble, two-state, differences in free energies, $\Delta G_{eq}^{(2)}$s, for zipping of the UUCG stem-loop, where the superscript denotes our assumption of the two-state model, using thermal melting experiments (Figure S3; see Materials and Methods). To determine the analogous $\Delta G_{eq}^{(2)}$s for zipping of the UUCG stem-loop using our smFET data, we applied a Gaussian mixture model (GMM)-based kinetic model (1) that identified two current states in our conductance trajectories. For the lowest temperature point of 35 °C, due to the very small population of the low-current state, a threshold was used, instead of a GMM, to distinguish between the two states (see Materials and Methods). Assuming that each state corresponded to a single RNA conformation, we were able to assign to the low- and high-current states to the unzipped $\boldsymbol{U}$ and the zipped $\boldsymbol{Z}$ conformations of the stem-loop (Figures 1 and S2). We note that the application of the GMM for the higher temperature points was made possible by an improved signal-to-noise ratio (SNR) of ~4–5 in this work relative to the SNR of ~3-4 that we have observed in our previous smFET studies of RNA stem-loops (2). This improvement could be attributed to several changes in the experimental design of the present work *versus* our previous work, including the use of a lower ionic strength buffer, resulting in reduced screening of the electrostatic charges on the RNA (3,4); the use of an RNA stem-loop construct where the conformational changes induced by zipping and unzipping were more proximal to the surface of the single-walled carbon nanotube (SWCNT); and the direct, covalent functionalization of the RNA stem-loop construct to the surface of the SWCNT (5-7) (Figure S1). These improvements over our previous work increased the change in current through the SWCNT during the conformational rearrangements of the RNA molecule, resulting in the higher SNR observed in the present work.

Using our GMM- and threshold-based kinetic models, we calculated the fractional occupancies of the $\boldsymbol{Z}$ and $\boldsymbol{U}$ conformations (f_Z and f_U, respectively) across the temperatures investigated here (Figure S2). In agreement with a previous study (2), f_U was observed to increase with increasing temperature, which is in line with the expectation that the unzipped $\boldsymbol{U}$ conformation should become more populated with increasing temperature (Table S3). These fractional occupancies were subsequently used to calculate the two-state equilibrium constants, $K_{eq}^{(2)}s$, for the zipping reaction and the corresponding two-state equilibrium free energies of zipping $\Delta G_{eq}^{(2)}$ (see Materials and Methods). The $\Delta G_{eq}^{(2)}$s for the smFET experiments were in striking agreement with those from the ensemble thermal melting experiments (Figure S4a and Table S3), validating that the current trajectories obtained from our smFET experiments report on the same zipping reaction that the ensemble thermal melting experiments report on.

Next, using the $K_{eq}^{(2)}$s estimated from the thermal melting experiments, we calculated the theoretical fractional occupancies of the $\boldsymbol{U}$ conformation for a given number of surface-tethered stem-loops over the range of experimental temperatures investigated here (Figure S4b). In the case of a single RNA stem-loop tethered to a single smFET device, f_U was directly calculated from $K_{eq}^{(2)}$ (see Materials and Methods).

For the case of multiple RNA stem-loops tethered to a single smFET device, we assumed that the $\boldsymbol{U}$ conformation corresponded to the scenario where at least one stem-loop was unzipped and the $\boldsymbol{Z}$ conformation corresponded to the case where all stem-loops were zipped. Given these assumptions, the expected fractional occupancy of the $\boldsymbol{U}$ conformation for this case was given by

$$f_U = 1 - f_Z^N,$$

where N denotes the number of tethered stem-loops and f_Z is the fractional occupancy of a single RNA stem-loop at a given temperature, which can be calculated from the ensemble $K_{eq}^{(2)}$ using

$$f_Z = \frac{K_{eq}^{(2)}}{1 + K_{eq}^{(2)}}.$$

Comparing the f_U values obtained from the GMM-based kinetic modeling employed to analyze for our experimentally obtained current trajectories with the f_U values that would be expected for various different numbers of surface-tethered RNA stem-loops allowed direct determination of the number of RNA stem-loops that generated a particular, experimentally obtained current trajectory. The results of this comparison showed that the f_U values we experimentally obtained overwhelmingly agree with the f_U values expected for the case in which a single RNA stem-loop is tethered to the surface of the SWCNT, confirming that our experimental conductance trajectories arose from a single, surface-tethered RNA molecule (Figure S4b). We note that the analysis described here may be used in the future as a general framework for directly determining the number of surface-tethered biomolecules on any smFET device.

Identification of the kinetic scheme between observed RNA conformations

To determine the kinetic scheme governing the zipping dynamics of the UUCG stem-loop, we made use of the fact that equilibrium changes in enthalpy and entropy (ΔH_{eq} and ΔS_{eq}, respectively) are thermodynamic state variables. Thus, for any two given states, these quantities should depend only on the identities of the states and not on the paths used to calculate them. We considered the two $\boldsymbol{U}$ conformations ($\boldsymbol{U^L}$ and $\boldsymbol{U^S}$) and two different paths connecting them, the 'direct' path A and the 'indirect' path B (Figure 2). For path A, $\Delta H_{eq}(\boldsymbol{U^L}, \boldsymbol{U^S})$ and $\Delta S_{eq}(\boldsymbol{U^L}, \boldsymbol{U^S})$ between these conformations, where $\boldsymbol{U^S}$ represents the initial conformation and $\boldsymbol{U^L}$ the final conformation, were calculated directly from the proportion of the slow and fast kinetic phases that corresponded to these $\boldsymbol{U}$ conformations (Figure S7c-d and Table S6; see Materials and Methods).

The indirect path B involves the two $\boldsymbol{Z}$ conformations ($\boldsymbol{Z^L}$ and $\boldsymbol{Z^S}$) (Figure 2). In this path, $\Delta H_{eq}(\boldsymbol{U^L}, \boldsymbol{U^S})$ and $\Delta S_{eq}(\boldsymbol{U^L}, \boldsymbol{U^S})$ can be expressed as differences between the $\boldsymbol{U}$ conformations

and the $\boldsymbol{Z}$ conformations, and between the $\boldsymbol{Z}$ conformations themselves (8). As above, $\Delta H_{eq}(\boldsymbol{Z^L}, \boldsymbol{Z^S})$ and $\Delta S_{eq}(\boldsymbol{Z^L}, \boldsymbol{Z^S})$ can be directly calculated based on the proportion of the slow and fast kinetic phases that corresponded to these $\boldsymbol{Z}$ conformations (Figure S7c-d and Table S6; see Materials and Methods). However, the ΔH_{eq}s (and ΔS_{eq}s) between the $\boldsymbol{U}$ and $\boldsymbol{Z}$ conformations cannot be calculated in a similar manner, because our dwell-time analysis (Figures S5 and S6) only yielded the rates of transitions out of a particular conformation and not the rates between two conformations (9). Instead, these rates yielded the activation parameters ($\Delta H^{\ddagger}$s and $\Delta S^{\ddagger}$) for transitions out of these conformations (Figure S7a-b and Table S7; see Materials and Methods). These $\Delta H^{\ddagger}$s and $\Delta S^{\ddagger}$ represented the corresponding changes between the $\boldsymbol{U}$,and between the $\boldsymbol{Z}$, conformations and the transition states ($\boldsymbol{TS}^{\ddagger}$s) for the transitions exiting these conformations (10). To calculate the corresponding ΔH_{eq}s and ΔS_{eq}s, we need to first specify how these $\boldsymbol{TS}^{\ddagger}$s fit into the kinetic scheme.

For kinetic scheme 1 (Figure 2a), we assume that the $\boldsymbol{TS}^{\ddagger}$ exiting out of $\boldsymbol{U^S}$ ($\boldsymbol{TS_1^{\ddagger}}$) corresponds to that out of $\boldsymbol{Z^S}$. We can then estimate the ΔH_{eq} and ΔS_{eq} between them as

$$\Delta H_{eq}(\boldsymbol{Z^S}, \boldsymbol{U^S}) = \Delta H^{\ddagger}(\boldsymbol{TS_1^{\ddagger}}, \boldsymbol{U^S}) - \Delta H^{\ddagger}(\boldsymbol{TS_1^{\ddagger}}, \boldsymbol{Z^S}) \text{ , and}$$

$$\Delta S_{eq}(\boldsymbol{Z^S}, \boldsymbol{U^S}) = \Delta S^{\ddagger}(\boldsymbol{TS_1^{\ddagger}}, \boldsymbol{U^S}) - \Delta S^{\ddagger}(\boldsymbol{TS_1^{\ddagger}}, \boldsymbol{Z^S}).$$

In this case, the other $\boldsymbol{TS}^{\ddagger}$ ($\boldsymbol{TS_2^{\ddagger}}$) out of $\boldsymbol{U^L}$ would correspond to that out of $\boldsymbol{Z^L}$, resulting in

$$\Delta H_{eq}(\boldsymbol{Z^L}, \boldsymbol{U^L}) = \Delta H^{\ddagger}(\boldsymbol{TS_2^{\ddagger}}, \boldsymbol{U^L}) - \Delta H^{\ddagger}(\boldsymbol{TS_2^{\ddagger}}, \boldsymbol{Z^L}) \text{ , and}$$

$$\Delta S_{eq}(\boldsymbol{Z^L}, \boldsymbol{U^L}) = \Delta S^{\ddagger}(\boldsymbol{TS_2^{\ddagger}}, \boldsymbol{U^L}) - \Delta S^{\ddagger}(\boldsymbol{TS_2^{\ddagger}}, \boldsymbol{Z^L}).$$

Thus, the 'indirect' $\Delta H_{eq}(\boldsymbol{U^L}, \boldsymbol{U^S})$ and $\Delta S_{eq}(\boldsymbol{U^L}, \boldsymbol{U^S})$ can be written as

$$\begin{aligned}\Delta H_{eq}(\boldsymbol{U^L}, \boldsymbol{U^S}) &= \Delta H_{eq}(\boldsymbol{Z^S}, \boldsymbol{U^S}) + \Delta H_{eq}(\boldsymbol{Z^L}, \boldsymbol{Z^S}) - \Delta H_{eq}(\boldsymbol{Z^L}, \boldsymbol{U^L}) \\ &= \Delta H^{\ddagger}\left(\boldsymbol{TS_1^{\ddagger}}, \boldsymbol{U^S}\right) - \Delta H^{\ddagger}\left(\boldsymbol{TS_1^{\ddagger}}, \boldsymbol{Z^S}\right) + \Delta H_{eq}(\boldsymbol{Z^L}, \boldsymbol{Z^S}) - \Delta H^{\ddagger}\left(\boldsymbol{TS_2^{\ddagger}}, \boldsymbol{U^L}\right) + \Delta H^{\ddagger}\left(\boldsymbol{TS_2^{\ddagger}}, \boldsymbol{Z^L}\right)\end{aligned}$$

and

$$\Delta S_{eq}(\boldsymbol{U^L}, \boldsymbol{U^S}) = \Delta S_{eq}(\boldsymbol{Z^S}, \boldsymbol{U^S}) + \Delta S_{eq}(\boldsymbol{Z^L}, \boldsymbol{Z^S}) - \Delta S_{eq}(\boldsymbol{Z^L}, \boldsymbol{U^L})$$
$$= \Delta S^{\ddagger}\left(\boldsymbol{TS_1^{\ddagger}}, \boldsymbol{U^S}\right) - \Delta S^{\ddagger}\left(\boldsymbol{TS_1^{\ddagger}}, \boldsymbol{Z^S}\right) + \Delta S_{eq}(\boldsymbol{Z^L}, \boldsymbol{Z^S}) - \Delta S^{\ddagger}\left(\boldsymbol{TS_2^{\ddagger}}, \boldsymbol{U^L}\right) + \Delta S^{\ddagger}\left(\boldsymbol{TS_2^{\ddagger}}, \boldsymbol{Z^L}\right).$$

In this scheme, by placing the $\boldsymbol{TS}^{\ddagger}$s in the above manner, we have assumed that transitions only occur between $\boldsymbol{U^S}$ and $\boldsymbol{Z^S}$, and between $\boldsymbol{U^L}$ and $\boldsymbol{Z^L}$ (Figure 2a).

Alternatively, in kinetic scheme 2 (Figure 2b), we assume that the $\boldsymbol{TS}^{\ddagger}$ exiting out of $\boldsymbol{U^S}$ ($\boldsymbol{TS_1^{\ddagger}}$) corresponds to that out of $\boldsymbol{Z^L}$, resulting in

$$\Delta H_{eq}(\boldsymbol{Z^L}, \boldsymbol{U^S}) = \Delta H^{\ddagger}(\boldsymbol{TS_1^{\ddagger}}, \boldsymbol{U^S}) - \Delta H^{\ddagger}(\boldsymbol{TS_1^{\ddagger}}, \boldsymbol{Z^L}) \text{ and}$$

$$\Delta S_{eq}(\boldsymbol{Z^L}, \boldsymbol{U^S}) = \Delta S^{\ddagger}(\boldsymbol{TS_1^{\ddagger}}, \boldsymbol{U^S}) - \Delta S^{\ddagger}(\boldsymbol{TS_1^{\ddagger}}, \boldsymbol{Z^L}) \ .$$

In this case, the other $\boldsymbol{TS}^{\ddagger}$ out of $\boldsymbol{U^L}$ ($\boldsymbol{TS_2^{\ddagger}}$) would correspond to that out of $\boldsymbol{Z^S}$, resulting in

$$\Delta H_{eq}(\boldsymbol{Z^S}, \boldsymbol{U^L}) = \Delta H^{\ddagger}(\boldsymbol{TS_2^{\ddagger}}, \boldsymbol{U^L}) - \Delta H^{\ddagger}(\boldsymbol{TS_2^{\ddagger}}, \boldsymbol{Z^S}) \text{ and}$$

$$\Delta S_{eq}(\boldsymbol{Z^S}, \boldsymbol{U^L}) = \Delta S^{\ddagger}(\boldsymbol{TS_2^{\ddagger}}, \boldsymbol{U^L}) - \Delta S^{\ddagger}(\boldsymbol{TS_2^{\ddagger}}, \boldsymbol{Z^S}) \ .$$

Thus, in this case, the 'indirect' ΔH_{eq} and ΔS_{eq} between $\boldsymbol{U^L}$ and $\boldsymbol{U^S}$ can be written as

$$\Delta H_{eq}(\boldsymbol{U^L}, \boldsymbol{U^S}) = \Delta H_{eq}(\boldsymbol{Z^L}, \boldsymbol{U^S}) - \Delta H_{eq}(\boldsymbol{Z^L}, \boldsymbol{Z^S}) - \Delta H_{eq}(\boldsymbol{Z^S}, \boldsymbol{U^L})$$
$$= \Delta H^{\ddagger}\left(\boldsymbol{TS_1^{\ddagger}}, \boldsymbol{U^S}\right) - \Delta H^{\ddagger}\left(\boldsymbol{TS_1^{\ddagger}}, \boldsymbol{Z^L}\right) - \Delta H_{eq}(\boldsymbol{Z^L}, \boldsymbol{Z^S}) - \Delta H^{\ddagger}\left(\boldsymbol{TS_2^{\ddagger}}, \boldsymbol{U^L}\right) + \Delta H^{\ddagger}\left(\boldsymbol{TS_2^{\ddagger}}, \boldsymbol{Z^S}\right)$$

and

$$\Delta S_{eq}(\boldsymbol{U^L}, \boldsymbol{U^S}) = \Delta S_{eq}(\boldsymbol{Z^L}, \boldsymbol{U^S}) - \Delta S_{eq}(\boldsymbol{Z^L}, \boldsymbol{Z^S}) - \Delta S_{eq}(\boldsymbol{Z^S}, \boldsymbol{U^L})$$
$$= \Delta S^{\ddagger}\left(\boldsymbol{TS_1^{\ddagger}}, \boldsymbol{U^S}\right) - \Delta S^{\ddagger}\left(\boldsymbol{TS_1^{\ddagger}}, \boldsymbol{Z^L}\right) - \Delta S_{eq}(\boldsymbol{Z^L}, \boldsymbol{Z^S}) - \Delta S^{\ddagger}\left(\boldsymbol{TS_2^{\ddagger}}, \boldsymbol{U^L}\right) + \Delta S^{\ddagger}\left(\boldsymbol{TS_2^{\ddagger}}, \boldsymbol{Z^S}\right).$$

In this scheme, with the above placement of the $\boldsymbol{TS}^{\ddagger}$s, we have assumed that transitions only occur between $\boldsymbol{U^S}$ and $\boldsymbol{Z^L}$, and between $\boldsymbol{U^L}$ and $\boldsymbol{Z^S}$ (Figure 2b).

While the two schemes differ only in how the $\boldsymbol{TS}^{\ddagger}$s, and thus the corresponding activation parameters, are arranged, we see that they lead to drastically different expressions for the indirect ΔH_{eq} and ΔS_{eq} between $\boldsymbol{U^S}$ and $\boldsymbol{U^L}$. By analyzing our experimentally obtained data in this way, we show that the zipping dynamics of the UUCG stem-loop are predominantly governed by kinetic scheme 1 (Figure 2).

References

1. Verma, A.R., Ray, K.K., Bodick, M., Kinz-Thompson, C.D. and Gonzalez, R.L., Jr. (2024) Increasing the accuracy of single-molecule data analysis using tMAVEN. *Biophys J*.
2. Jang, S.S., Dubnik, S., Hon, J., Hellenkamp, B., Lynall, D.G., Shepard, K.L., Nuckolls, C. and Gonzalez, R.L., Jr. (2023) Characterizing the Conformational Free-Energy Landscape of RNA Stem-Loops Using Single-Molecule Field-Effect Transistors. *Journal of the American Chemical Society*, **145**, 402-412.
3. Sorgenfrei, S., Chiu, C.Y., Johnston, M., Nuckolls, C. and Shepard, K.L. (2011) Debye screening in single-molecule carbon nanotube field-effect sensors. *Nano Lett*, **11**, 3739-3743.
4. Choi, Y., Olsen, T.J., Sims, P.C., Moody, I.S., Corso, B.L., Dang, M.N., Weiss, G.A. and Collins, P.G. (2013) Dissecting single-molecule signal transduction in carbon nanotube circuits with protein engineering. *Nano Lett*, **13**, 625-631.
5. Wilson, H., Ripp, S., Prisbrey, L., Brown, M.A., Sharf, T., Myles, D.J.T., Blank, K.G. and Minot, E.D. (2016) Electrical Monitoring of sp3 Defect Formation in Individual Carbon Nanotubes. *The Journal of Physical Chemistry C*, **120**, 1971-1976.
6. Vernick, S., Trocchia, S.M., Warren, S.B., Young, E.F., Bouilly, D., Gonzalez, R.L., Nuckolls, C. and Shepard, K.L. (2017) Electrostatic melting in a single-molecule field-effect transistor with applications in genomic identification. *Nat Commun*, **8**, 15450.
7. Lee, Y., Trocchia, S.M., Warren, S.B., Young, E.F., Vernick, S. and Shepard, K.L. (2018) Electrically Controllable Single-Point Covalent Functionalization of Spin-Cast Carbon-Nanotube Field-Effect Transistor Arrays. *ACS Nano*, **12**, 9922-9930.
8. Zumdahl, S.S. and Zumdahl, S.A. (2006) *Chemistry*. Cengage Learning.
9. Kinz-Thompson, C.D., Bailey, N.A. and Gonzalez, R.L., Jr. (2016) Precisely and Accurately Inferring Single-Molecule Rate Constants. *Methods Enzymol*, **581**, 187-225.
10. Fersht, A. (2017) *Structure and Mechanism in Protein Science*. WORLD SCIENTIFIC.

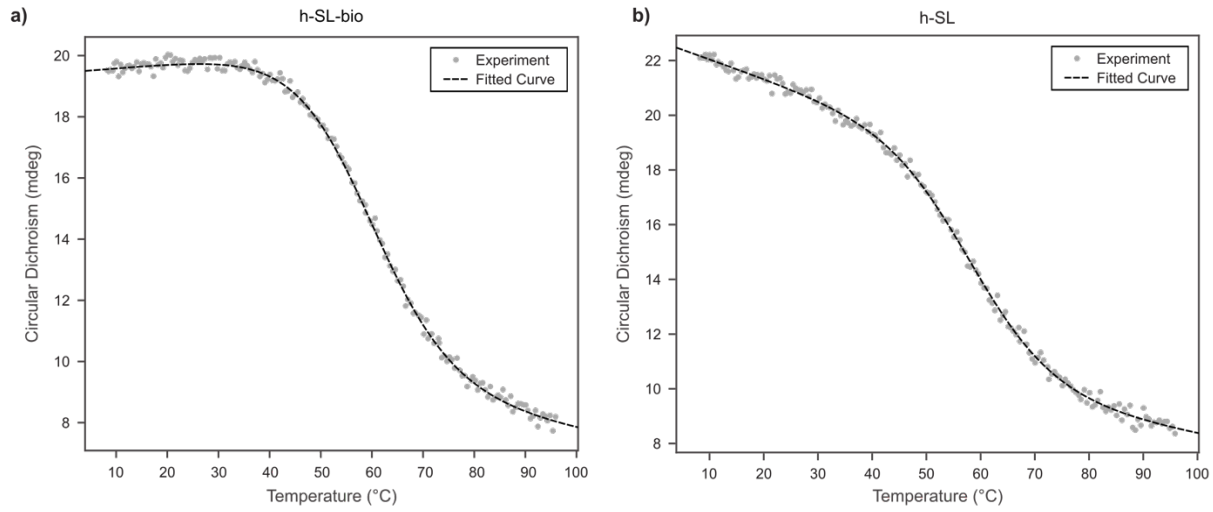

Figure S1. Thermal melting of the h-SL-bio and h-SL RNA stem-loop constructs. al melting curves showing the CD measured at 280 nm (gray circles) for the **(a)** h-SL-bio and **(b)** h-SL constructs as a function of temperature, along with the fit (black curve) to a two-state model of unimolecular transitions between the $\boldsymbol{U}$ and $\boldsymbol{Z}$ conformations.

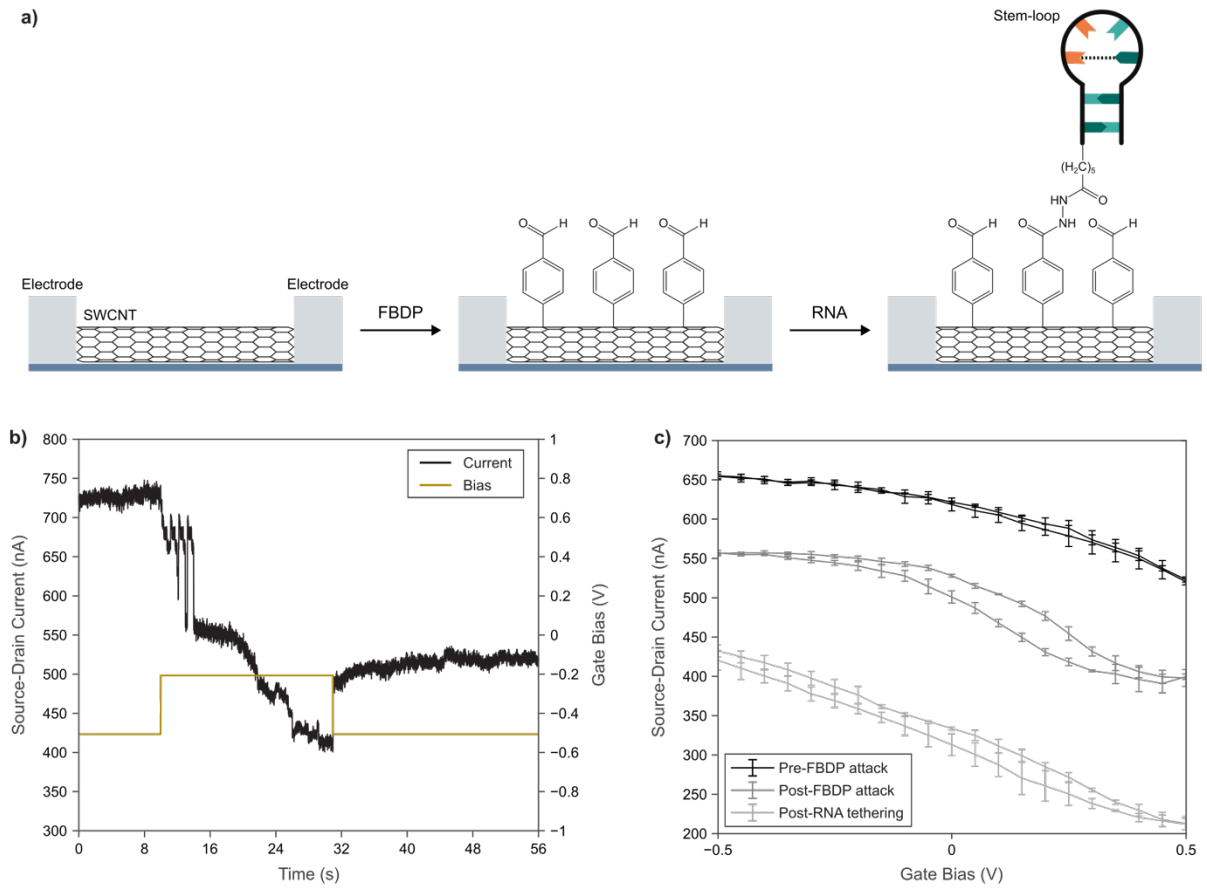

Figure S2. Covalent tethering of an RNA molecule to the surface of a SWCNT using an electrically controlled diazonium coupling reaction. (a) Schematic of the covalent tethering approach, showing first the tethering of FBDP onto the SWCNT surface through an electrically controlled diazonium reaction, followed by an RNA tethering step through a aldehyde-hydrazide coupling reaction. **(b)** I_{sd}-t (black) and V_{lg}-t (brown) measurements of an smFET device during the FBDP attack, showing multiple, clearly distinguished drops in current indicative of FBDP tethering when V_{lg} is ramped to −0.2 V from −0.5 V. **(c)** Average I_{sd}-V_{lg} curves for the same smFET device before FBDP attack, after FBDP attack, and after RNA tethering, measured in Recording Buffer. Error bars denote the standard deviation of three measurements.

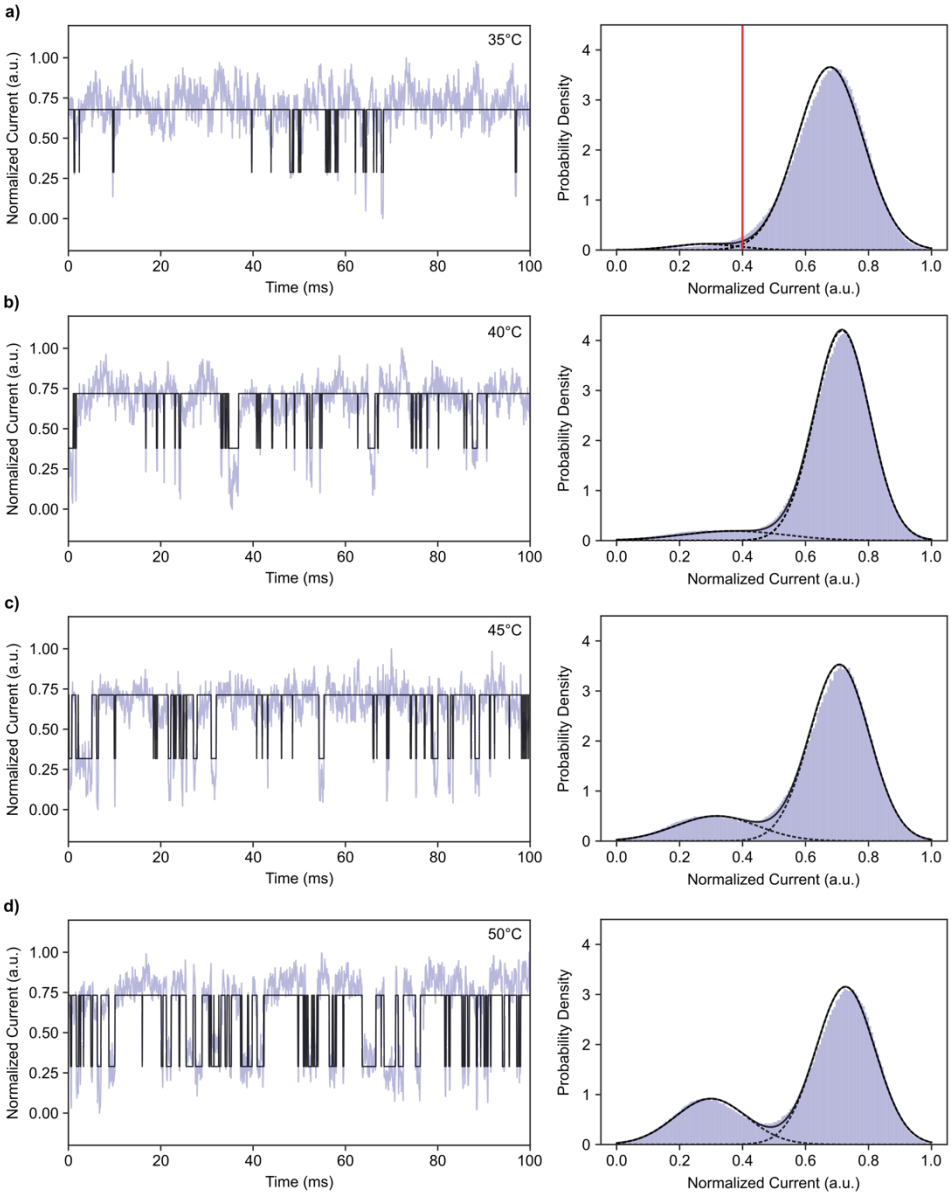

Figure S3. Temperature dependence of current trajectories recorded using the same, single UUCG stem-loop tethered onto the SWCNT surface of the same, single smFET device. smFET datasets obtained at **(a)** 35 °C, **(b)** 40 °C, **(c)** 45 °C, and **(d)** 50 °C showing (*left*) a representative 100-ms interval of the current trajectory (violet) overlaid with the idealized trajectory (black) and (*right*) a histogram of the current values across an entire 60 s trajectory (violet) overlaid with the inferred Gaussian density for each current state (dashed black curves) and the sum of all states (solid black curve) for the dataset at each temperature. The kinetic model that yielded these Gaussian distributions at 40 °C, 45 °C, and 50 °C were GMMs that were inferred from the data. For the 35 °C dataset, current values were first separated by a threshold value at 0.4 a.u. (red) and the means and standard deviations of the resulting populations yielded the individual Gaussian distributions for each state.

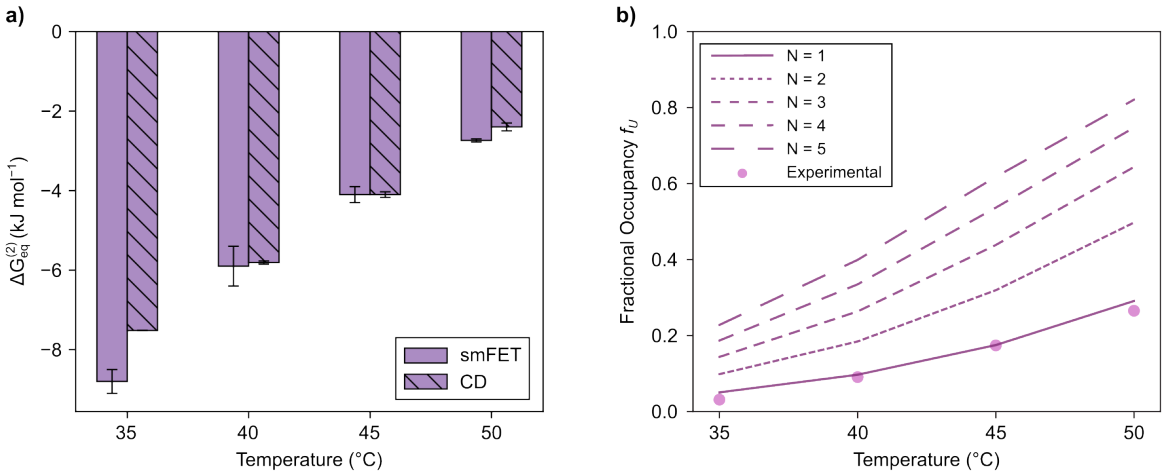

Figure S4. Confirmation that conductance trajectories report on the zipping dynamics of single, surface-tethered RNA stem-loops. (a) Comparisons of the $\Delta G^{(2)}_{eq}$s of zipping for the smFET (solid) and CD thermal melting (hatched) experiments. Error bars for the smFET experiments represent the standard deviations of the $\Delta G^{(2)}_{eq}$s calculated from three separate 20-s windows for the current trajectories at each temperature. Error bars for the CD thermal melting experiments represent the standard deviations of the $\Delta G^{(2)}_{eq}$s calculated from two independent experiments. **(b)** The expected fractional occupancies of the $\boldsymbol{U}$ conformation (f_U) at each temperature for a single tethered RNA stem-loop and various multiple tethered RNA stem-loop (lines) along with the f_U calculated from experimental smFET data (circles).

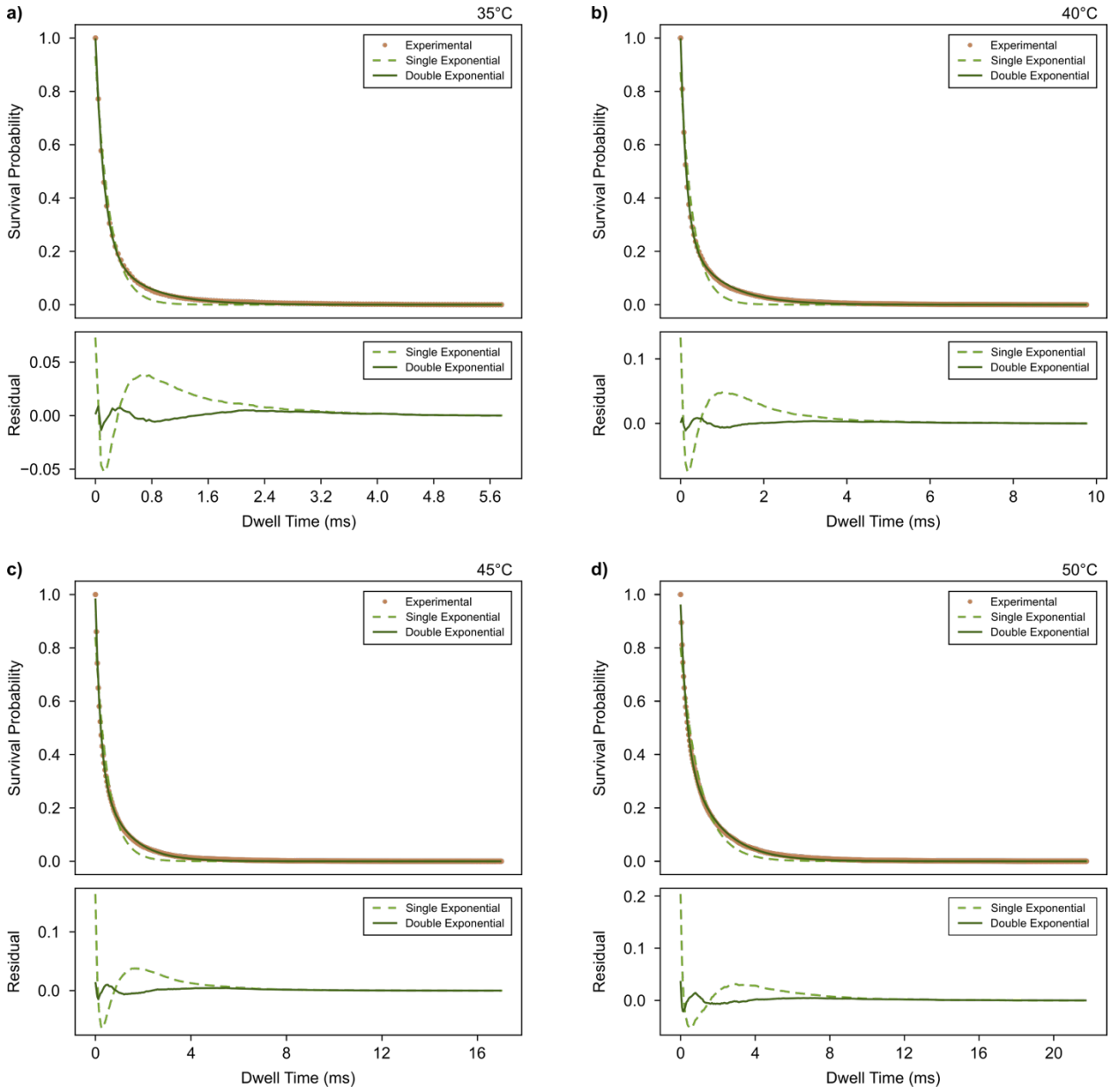

Figure S5. Kinetics of zipping. (*top*) Survival probabilities for the dwell-time distributions of the ***U*** conformation (circle) along with the single-exponential (dashed) and double-exponential (solid) fits and (*bottom*) the residuals of the single-exponential (dashed) and double-exponential (solid) fits for smFET datasets collected at **(a)** 35 °C, **(b)** 40 °C, **(c)** 45 °C, and **(d)** 50 °C.

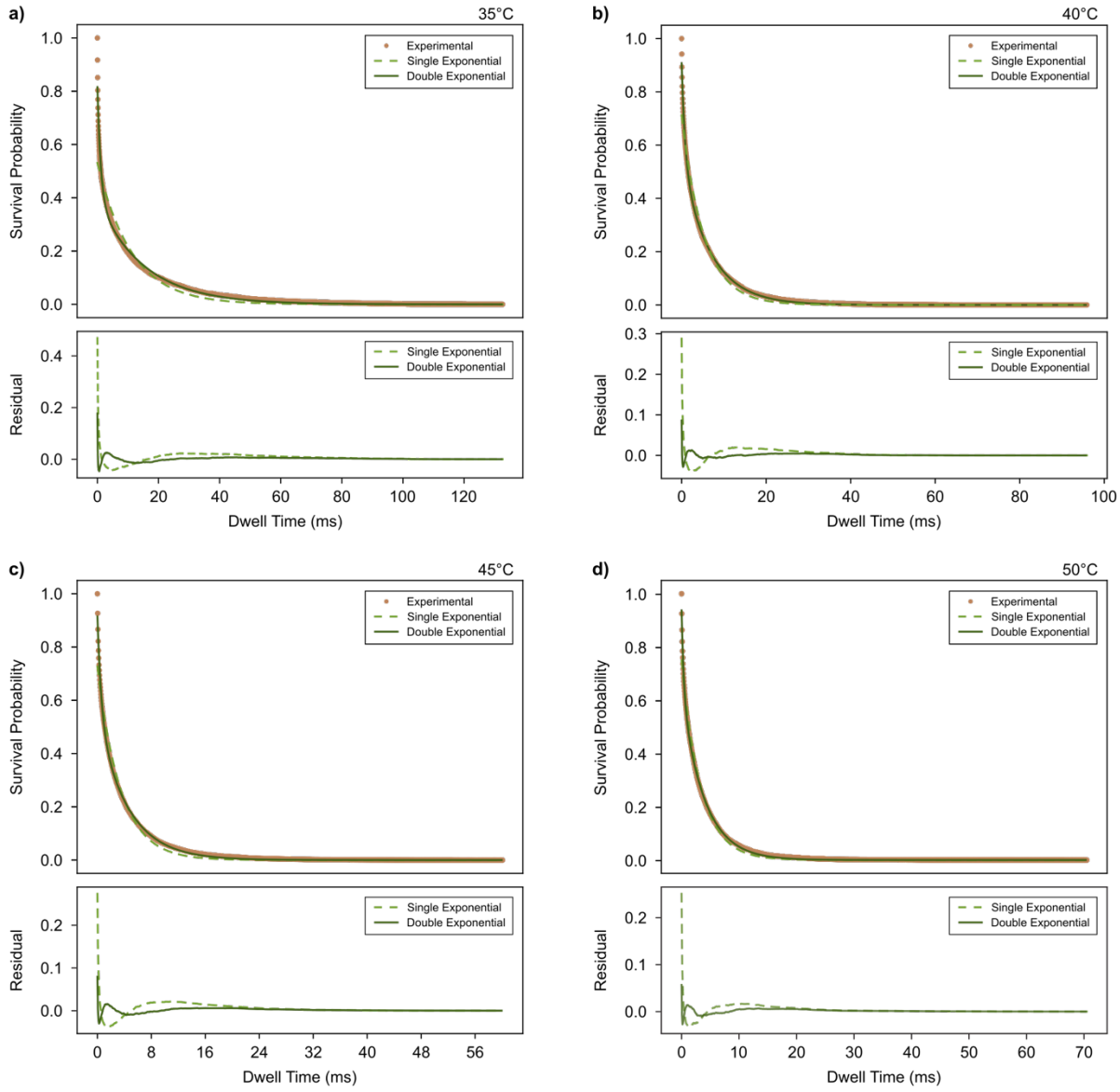

Figure S6. Kinetics of unzipping. (*top*) Survival probabilities for the dwell-time distributions of the ***Z*** conformation (circle) along with the single-exponential (dashed) and double-exponential (solid) fits and (*bottom*) the residuals of the single-exponential (dashed) and double-exponential (solid) fits for smFET datasets collected at **(a)** 35 °C, **(b)** 40 °C, **(c)** 45 °C, and **(d)** 50 °C.

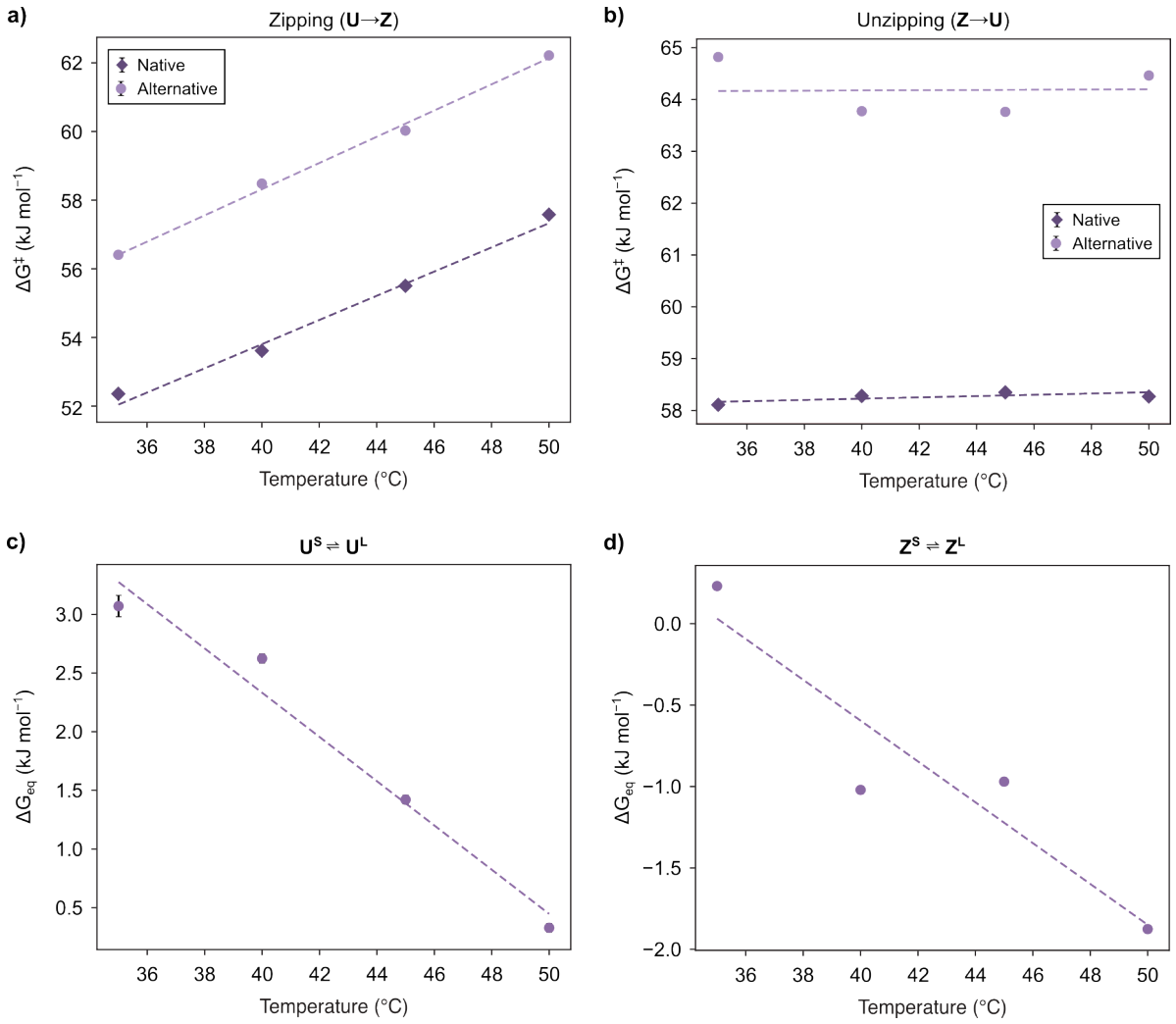

Figure S7. The activation and equilibrium free energies for the U and Z conformations. (a) Activation free energy of zipping ($\Delta \boldsymbol{G}^{\ddagger}$) as a function of temperature for the native (dark purple diamonds) and alternative (light purple circles) pathways along with linear fits to the data (dashed dark purple and dashed light purple lines, respectively). **(b)** Activation free energy of unzipping ($\Delta \boldsymbol{G}^{\ddagger}$) as a function of temperature for the native (dark purple diamonds) and alternative (light purple circles) pathways along with linear fits to the data (dashed dark purple and dashed light purple lines, respectively). **(c)** Equilibrium free energy ($\Delta \boldsymbol{G_{eq}}$) for the $\boldsymbol{U^S} \rightleftharpoons \boldsymbol{U^L}$ equilibrium as a function of temperature (circles) along with a linear fit to the data (dashed line). **(d)** Equilibrium free energy ($\Delta \boldsymbol{G_{eq}}$) for the $\boldsymbol{Z^S} \rightleftharpoons \boldsymbol{Z^L}$ equilibrium as a function of temperature (circles) along with a linear fit to the data (dashed line). Error bars in all plots represent the propagated error of the fit of the double-exponential decay function to the survival probability of the dwell-time distributions.

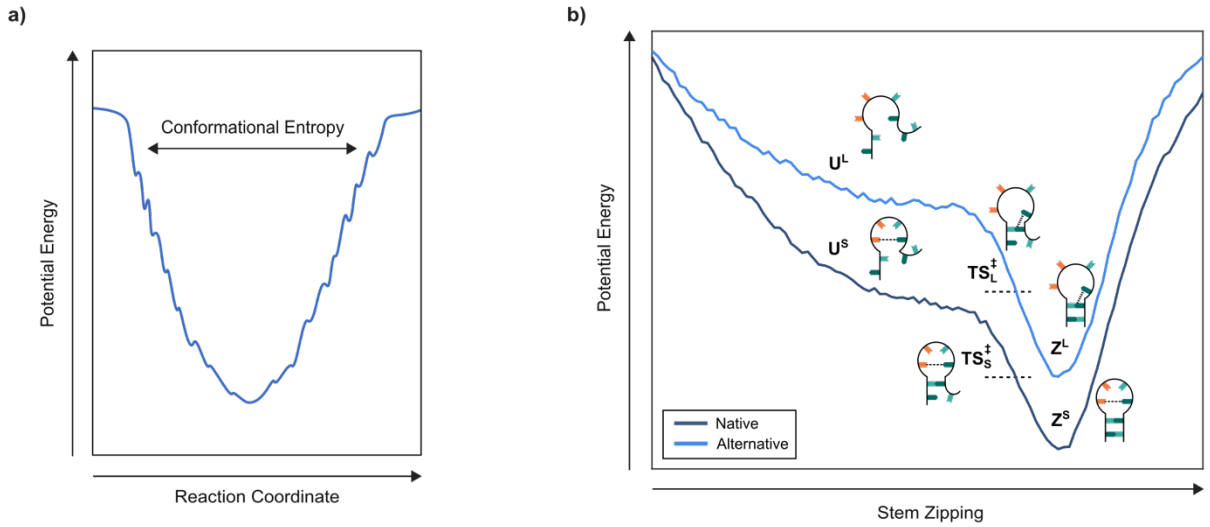

Figure S8. Potential energy landscapes. a) A hypothetical one-dimensional potential energy landscape for a biomolecule where each point corresponds to an individual biomolecular microstate projected along a relevant reaction coordinate. The height determines the potential energy, and the width of a well determines the conformational entropy of the state corresponding to the well. **b)** A one-dimensional representation of the two-dimensional UUCG stem-loop potential landscape (Figure 4a in the Main Text) projected along the reaction coordinate for stem zipping, showing the positions of the relevant UUCG stem-loop conformations and their structural representations.

Table S1. Sequences of the RNA stem-loop constructs.

Stem-loop Construct	Sequence
h-SL-bio	5’-hydrazide-GCUUCGGC-biotin-3’
h-SL	5’-hydrazide-GCUUCGGC-3’

Table S2. Thermodynamic parameters for the two-state model of RNA stem-loop zipping based on CD thermal melting experiments. Parameters from the fit of the set of parametric equations for two-state, unimolecular transitions between the $\boldsymbol{U}$ and $\boldsymbol{Z}$ conformations to the data from the CD thermal melting experiments. The parameters are the average of fitting results for two independently prepared samples and the errors are the standard deviations of the fitting results.

	$\Delta \boldsymbol{H}_{\boldsymbol{eq}}^{(2)}$ (kJ mol^{-1})	$\Delta \boldsymbol{S}_{\boldsymbol{eq}}^{(2)}$ (J mol^{-1}K^{-1})	$\Delta \boldsymbol{G}_{\boldsymbol{eq}}^{(2)}(\boldsymbol{37})$ (kJ mol^{-1})	$\boldsymbol{T}_{\boldsymbol{m}}$ (°C)
h-SL-bio	−113(2)	−342(8)	−6.84(0.01)	57.0(0.5)
h-SL	−115.7(0.2)	−351(1)	−7.0(0.2)	56.9(0.6)

Table S3. Comparison of thermodynamic parameters determined from smFET and CD thermal melting experiments. Errors (in parentheses) for the parameters obtained from the analysis of the smFET experiments represent the standard deviations of the parameters calculated from three separate 20-s windows for the current trajectories at each temperature. Error (in parentheses) for the parameters obtained from the analysis of the CD thermal melting experiments represent the standard deviations of the parameters calculated from two independent experiments.

	$\Delta G_{eq}^{(2)}$ (kJ mol^{-1})		f_U	
	smFET	CD	smFET	CD
35°C	−8.8(0.3)	−7.520(0.003)	0.031(0.004)	0.0504(0.0007)
40°C	−5.9(0.5)	−5.81(0.04)	0.09(0.02)	0.097(0.001)
45°C	−4.1(0.2)	−4.10(0.07)	0.17(0.01)	0.175(0.004)
50°C	−2.74(0.04)	−2.4(0.1)	0.265(0.003)	0.291(0.009)

Table S4. The two kinetic phases describing the zipping of the UUCG stem-loop. Errors (in parentheses) represent the error of the fit for the double-exponential decay function to the survival probability of the dwell-time distributions of the $\boldsymbol{U}$ conformations at each temperature.

	Slow phase		**Fast phase**	
	$k_{U\to Z}^{slow}$ (s^{-1})	$A_{U\to Z}^{slow}$	$k_{U\to Z}^{fast}$ (s^{-1})	$A_{U\to Z}^{fast}$
35°C	1740(40)	0.231(0.008)	8500(100)	0.767(0.008)
40°C	1130(10)	0.267(0.004)	7360(70)	0.732(0.004)
45°C	914(8)	0.363(0.004)	5060(60)	0.622(0.004)
50°C	584(4)	0.452(0.005)	3280(50)	0.511(0.004)

Table S5. The two kinetic phases describing the unzipping of the UUCG stem-loop. Errors (in parentheses) represent the error of the fit of the double-exponential decay function to the survival probability of the dwell-time distributions of the $\boldsymbol{Z}$ conformations at each temperature.

	Slow phase		**Fast phase**	
	$k_{Z\to U}^{slow}$ (s^{-1})	$A_{Z\to U}^{slow}$	$k_{Z\to U}^{fast}$ (s^{-1})	$A_{Z\to U}^{fast}$
35°C	65.2(0.3)	0.391(0.001)	900(10)	0.428(0.003)
40°C	148.2(0.4)	0.544(0.002)	1220(10)	0.367(0.002)
45°C	222.5(0.9)	0.542(0.003)	1720(30)	0.376(0.003)
50°C	252.9(0.7)	0.629(0.002)	2540(40)	0.313(0.003)

Table S6. Activation free energies, enthalpies, and entropies of the zipping and unzipping of the UUCG stem-loop along the native and alternative pathways. Errors (in parentheses) of the $\Delta \boldsymbol{G}^{\ddagger}$s are propagated from the corresponding transition rate constants. Errors for $\Delta \boldsymbol{H}^{\ddagger}$s and $\Delta \boldsymbol{S}^{\ddagger}$s represent the error of the fit of the linear function to the $\Delta \boldsymbol{G}^{\ddagger}$s as a function of absolute temperature.

		Zipping			Unzipping		
		$\Delta \boldsymbol{G}^{\ddagger}$ (kJ mol^{-1})	$\Delta H^{\ddagger}$ (kJ mol^{-1})	$\Delta S^{\ddagger}$ (J K^{-1} mol^{-1})	$\Delta \boldsymbol{G}^{\ddagger}$ (kJ mol^{-1})	$\Delta H^{\ddagger}$ (kJ mol^{-1})	$\Delta S^{\ddagger}$ (J K^{-1} mol^{-1})
Native Pathway	**35°C**	52.36(0.04)	−57(1)	−352(3)	58.11(0.03)	54(1)	−12(3)
	40°C	53.61(0.02)			58.28(0.03)		
	45°C	55.50(0.03)			58.35(0.04)		
	50°C	57.58(0.04)			58.27(0.04)		
Alternative Pathway	**35°C**	56.41(0.06)	−61.2(0.9)	−382 (3)	64.82(0.01)	63.5(0.2)	−2.1(0.7)
	40°C	58.48(0.03)			63.775(0.007)		
	45°C	60.03(0.02)			63.76(0.01)		
	50°C	62.22(0.02)			64.463(0.007)		

Table S7. Equilibrium free energies, enthalpies, and entropies for the two kinetic phases of zipping and unzipping of the UUCG stem-loop. Errors (in parentheses) of the $\Delta \boldsymbol{G_{eq}}$s are propagated from the corresponding ratio of pre-factors for the double-exponential decay. Errors for $\Delta \boldsymbol{H_{eq}}$s and $\Delta \boldsymbol{S_{eq}}$s represent the error of the fit of the linear function to the $\Delta \boldsymbol{G_{eq}}$s as a function of absolute temperature.

		ΔG_{eq} (kJ mol^{-1})	ΔH_{eq} (kJ mol^{-1})	ΔS_{eq} (J K^{-1} mol^{-1})
$\boldsymbol{U^S \rightleftharpoons U^L}$	**35°C**	3.07(0.09)	61(8)	190(20)
	40°C	2.62(0.04)		
	45°C	1.42(0.04)		
	50°C	0.33(0.04)		
$\boldsymbol{Z^S \rightleftharpoons Z^L}$	**35°C**	0.23(0.02)	40(10)	130(30)
	40°C	−1.02(0.02)		
	45°C	−0.97(0.02)		
	50°C	−1.88(0.02)		